Faithful effective-one-body waveforms of equal-mass coalescing black-hole binaries

Thibault Damour,[1,2] Alessandro Nagar,[1,2,3] Ernst Nils Dorband,[4] Denis Pollney,[4] and Luciano Rezzolla[4,5]

[1]*Institut des Hautes Etudes Scientifiques, 91440 Bures-sur-Yvette, France*

[2]*ICRANet, 65122 Pescara, Italy*

[3]*INFN, Sezione di Torino, Via Pietro Giuria 1, Torino, Italy*

[4]*Max-Planck-Institut für Gravitationsphysik, Albert-Einstein-Institut, Potsdam-Golm, Germany*

[5]*Department of Physics and Astronomy, Louisiana State University, Baton Rouge, Louisiana, USA*

(Received 18 December 2007; published 22 April 2008)

We compare a recently derived, *resummed* high post-Newtonian accuracy effective-one-body (EOB) quadrupolar waveform to the results of a numerical simulation of the *inspiral and merger* of an *equal-mass* black-hole binary. We find a remarkable agreement, both in phase and in amplitude, with a maximal dephasing which can be reduced below ± 0.005 gravitational-wave cycles over 12 gravitational-wave cycles corresponding to the end of the inspiral, the plunge, the merger, and the beginning of the ring-down. This level of agreement is shown for two different values of the effective fourth post-Newtonian parameter a_5, and for corresponding, appropriately flexed values of the radiation-reaction resummation parameter $v_{\rm pole}$. In addition, our resummed-EOB amplitude agrees to better than the 1% level with the numerical-relativity one up to the late inspiral. These results, together with other recent work on the EOB-numerical-relativity comparison, confirm the ability of the EOB formalism to accurately capture the general-relativistic waveforms.

DOI: 10.1103/PhysRevD.77.084017 PACS numbers: 04.25.Nx, 04.30.−w, 04.30.Db

I. INTRODUCTION

The gravitational-wave (GW) signals emitted by coalescing black-hole binaries are among the most promising targets for the currently operating network of ground-based detectors GEO/LIGO/VIRGO. The most useful part of the waveform for detection comes from the most relativistic part of the dynamics, around the coalescence, i.e. the last few cycles of the adiabatic inspiral, the plunge, and the merger. It is crucial for GW detection purposes to have available a large bank of ''*templates*'' that accurately represent the GW signals radiated by these binaries. The construction of *faithful*[1] GW templates for coalescing binaries comprising spinning black holes (with arbitrary masses m_1, m_2 and spins $\mathbf{S}_1$, $\mathbf{S}_2$) is a nontrivial task. In view of the multidimensionality of the corresponding parameter space, state-of-the-art numerical simulations cannot densely sample this parameter space. It is therefore urgent to devise *analytical* methods for computing (as a function of the physical parameters m_1, m_2, $\mathbf{S}_1$, $\mathbf{S}_2$) the corresponding GW waveforms. Here we continue the program of constructing, within the effective-one-body (EOB) method [2–5], high-accuracy analytic waveforms describing the GW signal emitted by inspiralling and merging binary black holes with arbitrary masses and spins. The EOB method was the first to provide estimates of the complete waveform (covering inspiral, plunge, merger, and ring-down) of a coalescing black-hole binary, both for nonspinning systems [3] and for spinning ones [6].

Numerical relativity (NR) recently succeeded in giving us access to reliable information about the dynamics and radiation of binary black-hole coalescences [7–18]. This opens the possibility of comparing the EOB predictions to NR results.

The comparison between the EOB approach and NR results has been recently initiated in several works [19–24]. These recent comparisons have been done using two different versions of EOB waveforms. The works of Buonanno *et al.* [19,20,23] use a *restricted waveform*, as proposed in the first EOB paper [3], but with an improved matching to the ring-down (similar to the one used in [25]) making use of three quasinormal modes. By contrast, the recent works of Damour and Nagar [22,24] use a new, *resummed* high post-Newtonian (PN) accuracy[2] EOB quadrupolar waveform. This improved EOB waveform has been shown to exhibit a remarkable agreement, both in phase and in amplitude, with NR waveforms in two separate physical situations: (i) inspiral and coalescence of small-mass-ratio (nonspinning) systems [22] (comparing it to waveforms computed by means of numerical simulations of test particles, with an added radiation-

[1]Following the terminology of [1], we recall that ''effectual templates'' are templates exhibiting large overlaps with an exact signal after maximizing over all (kinematical and dynamical) parameters, while ''faithful'' ones are so ''close'' to an exact one that they have large overlaps for values of the dynamical parameters which are very close to the real ones (''small biases'').

[2]This high-PN accuracy can be called 3^{+2}-PN because it includes not only the known comparable-mass 3PN waveform corrections, but also the test-mass limit of the 4PN and 5PN waveform amplitude corrections. See [24] for details and references.

reaction force, moving in black-hole backgrounds [26]) and (ii) inspiral (up to a limiting GW frequency $\sim 0.14/M$) of an equal-mass (nonspinning) system [24] (comparing it to recently published results of a high-accuracy inspiral simulation [18]).

The present paper is a continuation of the general program of constructing, within the EOB approach, high-accuracy, faithful analytic waveforms describing the gravitational-wave signal emitted by inspiralling and coalescing binary black holes. Here we shall consider the *coalescence signal* emitted by a nonspinning *equal-mass* binary black-hole system. We shall compare the phase and the amplitude of the new *resummed* 3^{+2}-PN-accurate EOB quadrupolar waveform of [22,24] to a numerical-relativity simulation of a coalescing black-hole binary performed at the Albert Einstein Institute (AEI).

This comparison will confirm the ability of the EOB approach to provide accurate analytical representations of NR waveforms. We note that the recent work [23] had already shown the ability of the analytically less accurate *restricted*[3] EOB waveforms to provide rather accurate approximations to NASA-Goddard NR coalescence waveforms for several different mass ratios ($m_1/m_2 = 1$, $3/2$, 2, and 4). More precisely, Ref. [23] found, in the equal-mass case, an EOB/NR dephasing of $\sim \pm 0.03$ GW cycles over 15 GW cycles. Concerning the amplitude, the latter reference does not quantify the restricted-EOB/NR difference, but one can read from Fig. 21 of [18] that the difference between the restricted PN (or EOB) amplitude and the Caltech-Cornell inspiral NR one is $\sim 7\%$. By contrast, the present paper will show that the new, resummed waveform exhibits a significantly smaller dephasing $\sim \pm 0.005$ GW cycles over 12 GW cycles, and, most remarkably, exhibits an excellent agreement in amplitude, both during the inspiral (where it is better than the 1% level) and the ring-down. This good result is obtained by making use (as proposed in several previous works [5,23,24,27,28]) of the natural *flexibility* of the EOB approach.

An alternative approach to the construction of analytical templates to model (nonspinning) coalescing binary black holes with arbitrary mass ratios has been recently proposed in Refs. [29,30].

This paper is organized as follows: In Sec. II we briefly describe the numerical simulation, whose results we use in the following. In Sec. III we spell out the features of the EOB waveform that we shall use. The main section is Sec. IV where we compare the new, resummed-EOB waveform to NR data. We also include a comparison where we use the less accurate restricted EOB waveform, and simpler quasinormal-mode (QNM) matching, used in some of the previous EOB works [3,19,20,23]. The paper ends with some conclusions.

[3]Here "restricted" refers to a waveform $h \propto \Omega^{2/3} e^{-2i\Phi}$.

II. BRIEF DESCRIPTION OF THE NUMERICAL SIMULATION

The numerical simulations have been carried out with the CCATIE code [31], a three-dimensional finite-differencing code developed at the Albert Einstein Institute and at the Center for Computation and Technology (CCT) of the Louisiana State University. The code is based on the CACTUS Computational Toolkit [32] for the solution of the Einstein equations in a finite-size domain covered with a Cartesian rectangular grid. The main and new features of the code have been recently discussed in Ref. [31], and here we briefly recall the most important ones only.

The Einstein equations are formulated as an initial-value problem via a conformal and traceless "3 + 1" decomposition. The spacetime geometry is decomposed into (i) the 3-metric of spacelike slices, (ii) the extrinsic curvature of those slices, and (iii) the lapse and shift. See [31] for the explicit form of the equations. The lapse function is evolved using the "1 + log" slicing condition [33], while the shift is evolved using the hyperbolic $\tilde{\Gamma}$-driver condition discussed in Ref. [34], but with the difference that advection terms have been added following the experience of [8,35], and are required for correct advection of the punctures in "moving-puncture" evolutions.

Spatial differentiation of the evolution variables is performed via straightforward finite differencing using fourth-order accurate centered stencils for all but the advection terms for each variable, which are instead upwinded in the direction of the shift. Vertex-centered adaptive mesh refinement is employed using nested grids via the CARPET infrastructure [36], with a 2:1 refinement for successive grid levels, and the highest resolution concentrated in the neighborhood of the individual horizons. Individual apparent horizons are located every few time steps during the time evolution [37], which is obtained via a "method of lines" and with a fourth-order accurate Runge-Kutta time integrator.

The simulations were performed on a domain with outer boundaries located at[4] $768M_c$, and a grid structure consists of nine mesh-refinement levels, the finest of which has a spatial resolution of $h = 0.02M_c$. Simulations with lower resolution (i.e., with $h = 0.024M_c$ and $h = 0.03M_c$) have also been carried out to validate the consistency of the results. An important feature of the CCATIE code is the possibility of employing two distinct methods for the calculation of the gravitational radiation produced. The first method uses the Newman-Penrose curvature scalar ψ_4, with respect to a suitable frame at the extraction radius. An alternative method measures the metric of the numerically generated spacetime against a fixed background at the

[4]We denote by M_c the internal length and mass units used in the code (with $G = c = 1$). Be aware that M_c slightly differs from $M = m_1 + m_2$ (see below).

TABLE I. For two different grid spacings h (first column), from left to right the columns report the following: initial ADM mass (scaled by $M = m_1 + m_2$) and ADM angular momentum of the spacetime (scaled by M^2); final mass (scaled by M) and dimensionless spin parameter $j_f = J_f/M_f^2$ of the merged black hole computed using the isolated/dynamical horizon formalism and from the fit of the ring-down; and dominant (quasinormal-mode) complex frequency of the ring-down.

h/M	$M_{\rm ADM}/M$	$J_{\rm ADM}/M^2$	$M_{\rm f}^{\rm hor}/M$	$j_{\rm f}^{\rm hor}$	$M_{\rm f}^{\rm ring}/M$	$j_{\rm f}^{\rm ring}$	$M\sigma_{2220}^{+}$
0.024	0.990 484	0.991 803	0.951 531	0.687 142	...	...	...
0.020	0.990 484	0.991 803	0.951 611	0.686 916	0.959 165	0.684 639	0.085 475 + i0.551 040

extraction radius, and determines the gauge-invariant Regge-Wheeler-Zerilli-Moncrief functions (see Ref. [38] for a review and references). Both methods have been systematically studied in Ref. [31], where they were also compared and shown to yield essentially identical results, both in terms of their asymptotic scaling properties (e.g., the peeling theorem), and in terms of the polarization amplitudes h_+ and $h_\times$. The analysis carried out here used as basic NR data the gauge-invariant (Zerilli-Moncrief) metric perturbations. These were extracted on (NR) coordinate 2-spheres with (NR) coordinate radii $R_{\rm NR} = 60M_c$ up to $R_{\rm NR} = 120M_c$, with a separation of $10M_c$ between two adjacent observers. The analysis carried out below uses, as an approximate asymptotic amplitude, the metric perturbation extracted at $R_{\rm NR} = 120M_c$.

The initial data for the black-hole binary are obtained by a Brill-Lindquist [39] construction, where the additional asymptotically flat end of each wormhole is compactified into a single point, the so-called *puncture* [40]. This approach explicitly uses the Bowen-York extrinsic curvature and solves the Hamiltonian constraint equation numerically (as detailed in Ref. [41]), after having chosen the free parameters for the puncture initial data. Quasicircularity of the initial orbit can then be obtained by specifying the puncture parameters in terms of an effective-potential method [42] as discussed in [31]. However, the assumption of "quasicircularity" (in the sense of [42]) at the (rather small) initial separations frequently used in numerical-relativity simulations has the drawback of introducing a small but nonzero amount of eccentricity. To compensate for, or reduce, this effect, other approaches have been suggested recently. One of these is based on an iterative minimization procedure where, throughout a series of simulations with slightly different initial black-hole configurations, the eccentricity is measured and minimized [43]. A simpler and rather effective approach has been proposed in Ref. [44], and consists of specifying the initial puncture parameters as the end state of a binary system whose evolution is determined, starting from a large separation, via the solution of the Taylor-expanded 3PN-accurate equations of motion [6,45,46].

Here we have essentially followed this latter prescription and considered, in particular, the initial data denoted by *E11* in Table I of [44], that have been shown there to reduce the eccentricity to $e < 0.002$. More specifically, our initial black holes have a coordinate distance $D = 11M_c$, momenta in the radial and tangential directions of $P_r = -7.094\,12 \times 10^{-4} M_c$ and $P_t = 0.090\,099\,3 M_c$, and a puncture mass parameter of $0.487\,035 M_c$, leading to initial individual black-hole masses $m_1 = m_2 = 0.499\,821 M_c$, and thus a total mass of the binary system $M = m_1 + m_2 = 0.999\,642 M_c$. Overall, the simulation covers about $\sim 1600M$ of the final evolution of the binary, thus comprising 8 orbits and about 16 GW cycles.

The mass and spin of the final black hole have been computed through two different methods yielding, however, very similar results: (i) by using the isolated/dynamical horizon formalism [47,48], where a proper rotational Killing vector is searched on the final apparent horizon to measure the spin, and the horizon area is used for computing the black-hole mass (see Sec. IV D of Ref. [31] for details); (ii) by performing a fit of the dominant quasinormal mode[5] of the *complex* ring-down waveform. This fit was performed by a nonlinear least-squares Gauss-Newton method, using $\exp(-\sigma t + \rho)$ as a parameter-dependent template [with two *complex* parameters (σ, ρ)], and an appropriate time interval during the ring-down (chosen by minimizing the post-fit residual). (For a discussion of methods for QNM fitting, see Refs. [49–51].) Then, from the best-fit value of σ (i.e., the QNM dominant complex frequency σ_{2220}^{+}), we computed the values of the mass and dimensionless spin parameters of the final black hole by using the interpolating fits given in Appendix E of Ref. [52]. The results of these two methods are denoted as $(M^{\rm hor}, j^{\rm hor})$ and $(M^{\rm ring}, j^{\rm ring})$, respectively.

The most relevant properties of the binary system are summarized in Table I. The difference (which is $\lesssim 1\%$) between the quoted values of the final black-hole parameters might come, in part, from inaccuracies in the interpolating fits of Ref. [52]. In the following we will use, in our EOB-matching procedure, the ring-down-fitted black-hole parameters $(M^{\rm ring}, j^{\rm ring})$ (so that the dominant complex frequency will be guaranteed to have the best possible value).

III. EOB METHOD AND WAVEFORM

We shall not review here in detail the EOB method [2–5], which has been described in several recent publications,

[5] In the notation introduced in Sec. III below, the dominant mode corresponds to the labels $(\pm, \ell, \ell', m, n) = (+, 2, 2, 2, 0)$.

notably Refs. [23,24]. We shall only indicate the EOB elements that are crucial for the present study. For detailed definitions of the EOB ingredients we refer to the recent paper [24] that we follow, except when otherwise indicated below.

Before entering the details of our EOB implementation, let us recall that Ref. [24] proposed a methodology for improving the waveform implementation of the EOB philosophy based on understanding, element by element, the physics behind each feature of the waveform, and on systematically comparing various EOB-based waveforms with "exact" waveforms obtained by numerical-relativity approaches. The first step of the methodology consisted in studying the small-mass-ratio limit, $\nu \equiv m_1 m_2/M^2 \ll 1$, in which one can use the well controllable "laboratory" of numerical simulations of test particles (with an added radiation-reaction force) moving in black-hole backgrounds. Historically, this laboratory has been important in understanding/discovering several key features of GW emission near black holes, a notable example of this being the work of Davis, Ruffini, and Tiomno [53] who discovered the transition between the plunge signal and a ringing tail when a particle falls into a black hole. The recent study of inspiralling and merging small-mass-ratio systems [22] led to introducing (and testing) the following improvements in EOB dynamics and waveforms: (i) an improved analytical expression for the $[(\ell, m) = (2, 2)$ even-parity Zerilli-Moncrief] waveform $\Psi_{22}^{(e)}$ which includes a resummation of the tail effects, and a 3^{+2}-PN-accurate "nonlinear" amplitude correction, (ii) the inclusion of nonquasicircular (NQC) corrections to the waveform, (iii) the inclusion of nonquasicircular corrections to radiation reaction, and (iv) an improved treatment of the matching between the plunge and ring-down waveforms which takes into account a new understanding of the importance of the number of QNMs, the sign of their frequencies, and the length of the interval on which the matching is done. The resulting improved implementation (when $\nu \ll 1$) of the EOB approach yielded very faithful waveforms whose amplitude and phase agreed remarkably well with the exact ones: in particular, the EOB phasing differed from the exact one by less than $\pm 1.1\%$ of a cycle over the whole process.

The program initiated in [22] was pursued in [24] where the comparable-mass version of the improved, resummed 3^{+2}-PN-accurate waveform was compared with the recently published inspiral simulation of the Caltech-Cornell group [18]. It was found that, by exploiting the combined flexibility in a_5 and $v_{\rm pole}$, one could reach a remarkable phase agreement, better than 0.001 GW cycles over 30 GW cycles. Here, we shall similarly exploit the flexibility in a_5 and $v_{\rm pole}$ to best fit the AEI merger waveform.

Let us recall that the EOB approach is a *nonperturbatively resummed* analytic technique which consists of several different elements:

(i) A *Hamiltonian* $H_{\rm real}$ describing the conservative part of the relative two-body dynamics. The key ingredient of this Hamiltonian [defined in Eqs. (13) and (14) of [24]] is the "radial potential" $A(r)$.[6] This radial potential is defined, at n-PN order, as the (1, n) Padé resummation [4] of its Taylor (i.e. usual PN) expansion [written in Eq. (15) of [24]].

(ii) A *radiation-reaction force* $\mathcal{F}_\varphi$ (denoted $\hat{\mathcal{F}}_\varphi$ after its rescaling by $1/\mu$), which is defined as a Padé resummation [1] of its Taylor expansion. See Eq. (17) of [24] where $f_{\rm DIS}$ is the P_4^4 Padé resummation of $(1 - v/v_{\rm pole})\hat{F}^{\rm Taylor}(v; \nu)$. The coefficients of $\hat{F}^{\rm Taylor}$ in Eq. (18) of [24] have been derived in Refs. [54–59]. We shall also consider at the end, following Ref. [22], the possibility of modifying $\mathcal{F}_\varphi$ by a *nonquasicircular* correcting factor, Eq. (13).

(iii) *Improved "post-post-circular"* dynamical initial data (positions and momenta) as advocated in Sec. III B of [24]. To explain the improved construction of initial data let us introduce a formal bookkeeping parameter ε (to be set to 1 at the end) in front of the radiation reaction $\hat{\mathcal{F}}_\varphi$ in the EOB equations of motion. One can then show that the quasicircular inspiralling solution of the EOB equations of motion formally satisfies

$$p_\varphi = j_0(r) + \varepsilon^2 j_2(r) + O(\varepsilon^4), \tag{1}$$

$$p_{r_*} = \varepsilon \pi_1(r) + \varepsilon^3 \pi_3(r) + O(\varepsilon^5). \tag{2}$$

Here, $j_0(r)$ is the usual *circular* approximation to the inspiralling angular momentum as explicitly given by Eq. (4.5) of [3], while the order ε ("post-circular") term $\pi_1(r)$ is obtained by (i) inserting the circular approximation $p_\varphi = j_0(r)$ on the left-hand side (l.h.s.) of Eq. (10) of [21], (ii) using the chain rule $dj_0(r)/dt = (dj_0(r)/dr)(dr/dt)$, (iii) replacing dr/dt by the right-hand side (r.h.s.) of Eq. (9) of [21], and (iv) solving for p_{r_*} at the first order in ε. This leads to an explicit result of the form (using the notation defined in Ref. [21])

$$\varepsilon \pi_1(r) = \left[\nu \hat{H} \hat{H}_{\rm eff} \left(\frac{B}{A}\right)^{1/2} \left(\frac{dj_0}{dr}\right)^{-1} \hat{\mathcal{F}}_\varphi \right]_0, \tag{3}$$

where the subscript 0 indicates that the r.h.s. is evaluated at the leading circular approximation $\varepsilon \to 0$. The post-circular EOB approximation (j_0, π_1) was introduced in Ref. [3] and then used in most of the

[6]Except when said otherwise, we henceforth systematically scale dimensionful quantities by means of the total rest mass $M \equiv m_1 + m_2$ of the binary system. For instance, we use the dimensionless EOB radial coordinate $r \equiv R_{\rm EOB}/M$, with $G = 1$. Note also that $\nu \equiv \mu/M$ with $\mu \equiv m_1 m_2/M$.

subsequent EOB papers [6,19,21,23,23,26]. The *post-post-circular* approximation (order ε^2), introduced in Ref. [24] and used here, consists of (i) formally solving Eq. (11) of [21] with respect to the explicit p_φ^2 appearing on the r.h.s., (ii) replacing p_{r_*} by its post-circular approximation (3), (iii) using the chain rule $d\pi_1(r)/dt = (d\pi_1(r)/dr)(dr/dt)$, and (iv) replacing dr/dt in terms of π_1 (to leading order) by using Eq. (9) of [21]. The result yields an explicit expression of the type $p_\varphi^2 \simeq j_0^2(r)[1 + \varepsilon^2 k_2(r)]$ of which one finally takes the square root. In principle, this procedure can be iterated to get initial data at any order in ε. We found that the post-post-circular initial data $(j_0\sqrt{1+\varepsilon^2 k_2}, \pi_1)$ are sufficient to lead to negligible eccentricity when starting the integration of the EOB equations of motion at radius $r = 15$.

(iv) An improved, resummed *"inspiral-plus-plunge"* (hereafter abbreviated as *"insplunge"*) *waveform*[7] of the form

$$\left(\frac{c^2}{GM}\right)\Psi_{22}^{\rm insplunge}(t) = -4\sqrt{\frac{\pi}{30}}\nu(r_\omega\Omega)^2 f_{22}^{\rm NQC} F_{22} e^{-2i\Phi}, \tag{4}$$

where $\Phi(t)$ is the EOB orbital phase, $\Omega = \dot{\Phi}$ is the EOB orbital frequency, and $r_\omega \equiv r\psi^{1/3}$ is a modified EOB radius, with ψ being defined in Eq. (22) of Ref. [25]. The factor F_{22} is a resummed, 3^{+2}-PN-accurate complex amplitude correction valid during the (adiabatic) inspiral, and $f_{22}^{\rm NQC}$ is an extra complex correcting factor, aimed at taking care (in an effective way) of various *nonquasicircular* effects during the plunge. F_{22} is defined in Eqs. (5)–(11) of [24], with f_{22} being the (3, 2) Padé resummation of $f_{22}^{\rm Taylor}$ [see also Ref. [60] for an independent derivation of the nonresummed, 3PN-accurate (2, 2) waveform].

(v) A *ring-down waveform*

$$\Psi_{22}^{\rm ringdown}(t) = \sum_N C_N^+ e^{-\sigma_N^+ t} + \sum_N C_N^- e^{-\sigma_N^- t}, \tag{5}$$

where the label N actually refers to a set of indices (ℓ, ℓ', m, n), with $(\ell, m) = (2, 2)$ being the Schwarzschild-background multipolarity degrees of the considered (Zerilli-Moncrief-type) waveform $\Psi_{\ell m} \sim h_{\ell m}$, with $n = 0, 1, 2, \ldots$ being the "overtone number" of the considered Kerr-background quasinormal mode ($n = 0$ denoting the fundamental mode), and ℓ' the degree of its associated spheroidal harmonics $S_{\ell' m}(a\sigma, \theta)$. In addition $\sigma_N^\pm = \alpha_N^\pm \pm i\omega_N^\pm$ refers to the positive/negative complex QNM frequencies ($\alpha_N^\pm > 0$ and $\omega_N^\pm > 0$ indicate the inverse damping time and the oscillation frequency of each mode, respectively). The sum over ℓ' comes from the fact that an ordinary spherical harmonics $Y_{\ell m}(\theta, \phi)$ (used as an expansion basis to define $\Psi_{\ell m}$) can be expanded in the spheroidal harmonics $S_{\ell' m}(a\sigma, \theta)e^{im\phi}$ characterizing the angular dependence of the Kerr-background QNMs [61].

(vi) An improved way of *matching* the inspiral-plus-plunge waveform to the ring-down one, on a $(2p + 1)$-tooth "comb" $(t_m - p\delta, t_m - (p-1)\delta, \ldots, t_m - \delta, t_m, t_m + \delta, \ldots, t_m + p\delta)$, of total length $\Delta t = 2p\delta$, which is centered around some "matching" time t_m. Below we will fix the integer p to the value $p = 2$, corresponding to five matching points.

(vii) Finally, we define our complete EOB matched waveform (from $t = -\infty$ to $t = +\infty$) as

$$\Psi_{22}^{\rm EOB}(t) \equiv \theta(t_m - t)\Psi_{22}^{\rm insplunge}(t) + \theta(t - t_m)\Psi_{22}^{\rm ringdown}(t) \tag{6}$$

where $\theta(t)$ denotes Heaviside's step function. Note that, if one wanted to have a C^∞ transition between the two waveforms, one could replace $\theta(t - t_m)$ by one of Laurent Schwartz's well-known smoothed step functions (or "partitions of unity") $\theta_\varepsilon((t - t_m)/(2p\delta))$.

Let us now state the specific choices made here for the various EOB ingredients just recalled. Some of these choices correspond to various ways of "flexing" the EOB formalism (in the sense of Ref. [27]).

(i) We "flex" the currently known 3PN-accurate EOB Hamiltonian [4,45] by introducing an (effective) 4PN Hamiltonian parameter a_5, parametrizing an additional contribution $+a_5\nu/r^5$ in the main EOB radial function $A(r)$. This parameter has already been introduced (under varying notations) in several previous works [5,23,24,27,28].

(ii) Similarly, the EOB radiation-reaction force [defined by Eq. (17) of [24]] is "flexed" by allowing the Padé-resummation parameter $v_{\rm pole}$ to differ from the "standard" value $v_{\rm pole}^{\rm DIS}(\nu)$ advocated in [1].

In addition, we shall also briefly explore another physically natural flexibility in the radiation reaction, which was introduced (and shown to be physically needed for faithfulness) in [22]: the multiplication of the radiation reaction by a NQC correction factor $f_{\rm RR}^{\rm NQC}$; see Eq. (13) below.

[7]Here, as before, we work with a *metric-level* ("h"), rather than *curvature-level* ("ψ_4") waveform. However, we normalize here this metric waveform in the same "Zerilli-Moncrief" way as in the test-mass work [22]. This differs simply by a numerical factor from both the usual tensor-spherical harmonics (ℓ, m) metric amplitude $h_{\ell m}$ and the related metric variables $Q_{\ell m}^{+,\times}$ extracted from the NR evolution [31]: $Rh_{\ell m} = \sqrt{(\ell+2)(\ell+1)\ell(\ell-1)}(\Psi_{\ell m}^{(e)} + i\Psi_{\ell m}^{(o)}) = \frac{1}{\sqrt{2}}(Q_{\ell m}^+ - i\int_{-\infty}^t Q_{\ell m}^\times(t')dt')$.

(iii) To define precisely the "insplunge waveform" (4) we need to specify the following:
   (a) The argument $x(t)$ used in the f_{22} "brick" within F_{22} [see Eq. (10) of [24]]. We shall use here $x = \Omega^{2/3}$ where Ω is the *EOB orbital frequency*.
   (b) The Padé resummation of the Taylor expansion $f_{22}^{\rm Taylor}$ of f_{22}. As in [24] we shall use a P_2^3 Padé.
   (c) The definition of the NQC correction factor $f_{22}^{\rm NQC}$. To do this we follow the rationale explained in [22]. For convenience, we choose (as suggested in footnote 9 of [22]) a *factorized* complex NQC factor

$$f_{22}^{\rm NQC} = \left[1 + a\frac{p_{r_*}^2}{(r\Omega)^2 + \epsilon}\right]\exp\left(+{\rm i}b\frac{p_{r_*}}{r\Omega}\right), \tag{7}$$

in which a (denoted a' in the cited footnote) affects only the modulus, and b (alias b') only the phase. To ease some technical problems during the ring-down linked to the fact that $\Omega(t)$ tends exponentially towards zero as $t \to +\infty$, we have added a ("cutoff") constant ϵ to the first denominator $(r\Omega)^2$. As discussed in [22], one can *a priori* analytically determine a "good" value of the NQC-modulus parameter a by requiring that the modulus of the full EOB insplunge waveform (4) be maximum at the "EOB light ring," i.e. when the EOB orbital frequency Ω reaches a maximum. Reference [22] mentioned that, in the $\nu \ll 1$ limit, this requirement implied $a = 1/2$ (when $\epsilon = 0$). We found, by numerically exploring the modulus of $\Psi_{22}^{\rm insplunge}(t)$, that the same value, $a = 1/2$ (together with $\epsilon = 0.12$), can be used in the case $\nu = 1/4$ considered here. Concerning the NQC-phase parameter b we simply choose $b = 0$. [Note that the comparable-mass resummed-EOB waveform of [24] uses a refined estimate for the additional phase δ_{22} of $\Psi_{22}^{\rm insplunge}(t)$ compared to the one used in [22].]

(iv) Concerning the choice of QNMs, we recall that the discussion of the physical excitation of QNMs in [22] (see the summary in Fig. 4 there) suggested that it is sufficient to use only *positive-frequency* QNMs in the ring-down waveform (5). This is what we shall do here as well.
A new feature of the comparable-mass case (with respect to the small ν limit) is the "mixing" between various ℓ' QNMs (with $\ell' \neq \ell$) that can enter a given (ℓ, m) multipolar wave. This mixing is due to the "$a\omega$ coupling" terms in the separated Teukolsky equations and has been discussed in [19,61]. However, as emphasized in [19], this coupling has only a small effect on the $(\ell, m) = (2, 2)$ waveform. We shall neglect it and consider only the (positive-frequency) QNM modes having the same values of (ℓ, m) as the considered multipolar waveform $h_{\ell m}$ [i.e. (2, 2) in the present paper].
On the other hand, contrary to other recent implementations of the EOB approach [19,20,23], we shall use a matching comb with *five* teeth ($p = 2$) and *five* (positive-frequency) QNMs $\sigma_{\ell mn}^+ = \alpha_{\ell mn}^+ + {\rm i}\omega_{\ell mn}^+$, with $\ell = 2$, $m = +2$, and $n = 0, 1, 2, 3, 4$. To estimate the values (as functions of the mass and spin of the final black hole) of the damping time and the oscillation frequency of each mode, we did the following: (i) for the first three modes we used the approximate fitting formulas given in Appendix E of Ref. [52]; while, (ii) for the fourth and fifth modes (i.e. $n = 3, 4$) we noticed that the graphic results of [62] (notably his most relevant Fig. 4) exhibit an *approximate linearity* of the complex QNM frequency $\sigma_{\ell mn}^+$ as a function of the overtone number n. (Indeed, the corresponding points in the complex σ plane are approximately aligned.) We then exploited this approximate linearity to express the needed $n = 3$ and $n = 4$ complex frequencies as linear combinations of the above-discussed $n = 1$ and $n = 2$ ones.

(v) Concerning the *matching*, on a multitoothed comb, of the inspiral-plus-plunge waveform to the ring-down one, we need to specify the two parameters defining such a comb, namely, the central "matching" time t_m, and the spacing between the teeth of the comb: $\delta = \Delta t/4$.[8] In conformity with the basic idea proposed in the original EOB paper [3], we choose as central matching time t_m the so-called "EOB light-ring crossing" time, i.e., the EOB dynamical time when the EOB orbital frequency Ω reaches its maximum. See [22] for a detailed discussion of why such a choice is physically preferred. Concerning the choice of the comb spacing δ, we expect from [22] that a value of order $\delta = (7.2M)/4 = 1.8M$ will be good. Below, we shall explore values near this one.

IV. COMPARING THE NR WAVEFORM TO EOB ONES

As explained in Sec. II, the basic NR data that we shall consider are a time series giving the quadrupolar [$(\ell, m) = (2, 2)$, Zerilli-Moncrief-normalized] metric waveform $\Psi_{22}^{\rm NR}$

[8] Note that in [22] we used the letter δ to denote the full width Δt of the comb.

as a function of the NR time variable[9] $t_{\rm NR}$ (measured in units of $M \equiv m_1 + m_2$). $\Psi^{\rm NR}_{22}(t_{\rm NR})$ is a complex number. The NR results consist of the real and imaginary parts of $\Psi^{\rm NR}_{22}$. It is, however, more convenient to decompose the complex waveform in modulus (or amplitude) and phase, say,

$$\Psi^{\rm NR}_{22}(t_{\rm NR}) = A^{\rm NR}_{22}(t_{\rm NR}) \exp(-{\rm i}\phi^{\rm NR}_{22}({\rm t}_{\rm NR})). \tag{8}$$

The 2π ambiguity in the phase is fixed by starting with the principal value of the argument of $\Psi^{\rm NR}_{22}$ at the beginning of the NR simulation, and then keeping track of the 2π turns as the waveform continuously unfolds.

One can then compute the GW frequency as a function of time by (numerically) differentiating the GW phase

$$\omega^{\rm NR}_{22}(t_{\rm NR}) = \frac{d\phi^{\rm NR}_{22}}{dt_{\rm NR}}. \tag{9}$$

[It can equivalently be obtained by computing the imaginary part of the logarithmic time derivative of $\Psi^{\rm NR}_{22}(t_{\rm NR})$.]

As emphasized in [24], another useful diagnostic of GW radiation is the GW phase acceleration $\alpha = d\omega/dt = d^2\phi/dt^2$ considered as a function of the GW frequency ω. However, because of the presence of some additional high-frequency wiggles in ϕ and ω in the NR data, we shall not consider here the phase-acceleration curve $\alpha(\omega)$. Instead, we shall directly compare the numerical GW amplitude, phase, and frequency to their analytical, EOB counterparts.

The integration of the basic EOB dynamical equations (written in [24]) gives, for each chosen value of the EOB "flexibility parameters" (notably a_5 and $\nu_{\rm pole}$), several important time series, and notably (i) the EOB orbital frequency $\Omega(t_{\rm EOB})$, where $t_{\rm EOB}$ is the EOB dynamical time scale (measured in units of M), and (ii) the new, resummed *matched* 3^{+2}-PN-accurate quadrupolar EOB waveform $\Psi^{\rm EOB}_{22}(t_{\rm EOB})$; then, from the latter, one can define (as for the NR case) the corresponding EOB amplitude $A^{\rm EOB}_{22}(t_{\rm EOB})$, EOB phase $\phi^{\rm EOB}_{22}(t_{\rm EOB})$, and EOB frequency $\omega^{\rm EOB}_{22}(t_{\rm EOB})$. To compare the NR and EOB phase time series $\phi^{\rm NR}_{22}(t_{\rm NR})$ and $\phi^{\rm EOB}_{22}(t_{\rm EOB})$, one needs to shift, by additive constants, both one of the time variables and one of the phases. In other words, we need to determine τ and α such that the "shifted" EOB quantities

$$t'_{\rm EOB} = t_{\rm EOB} + \tau, \qquad \phi'^{\rm EOB}_{22} = \phi^{\rm EOB}_{22} + \alpha \tag{10}$$

"best fit" the NR ones. One convenient way to do so is first to "pinch" the EOB/NR phase difference at two different instants (corresponding to two different frequencies). More precisely, one can choose two NR times $t^{\rm NR}_1$, $t^{\rm NR}_2$, which determine two corresponding GW frequencies[10] $\omega_1 = \omega^{\rm NR}_{22}(t^{\rm NR}_1)$, $\omega_2 = \omega^{\rm NR}_{22}(t^{\rm NR}_2)$, and then find the time shift $\tau(\omega_1, \omega_2)$ such that the shifted EOB phase difference, between ω_1 and ω_2, $\Delta\phi^{\rm EOB}(\tau) \equiv \phi'^{\rm EOB}_{22}(t'^{\rm EOB}_2) - \phi'^{\rm EOB}_{22}(t'^{\rm EOB}_1) = \phi^{\rm EOB}_{22}(t^{\rm EOB}_2 + \tau) - \phi^{\rm EOB}_{22}(t^{\rm EOB}_1 + \tau)$ is equal to the corresponding (unshifted) NR phase difference $\Delta\phi^{\rm NR} \equiv \phi^{\rm NR}_{22}(t^{\rm NR}_2) - \phi^{\rm NR}_{22}(t^{\rm NR}_1)$. This yields one equation for one unknown (τ), and (uniquely) determines a value $\tau(\omega_1, \omega_2)$ of τ. (Note that the $\omega_2 \to \omega_1 = \omega_m$ limit of this procedure yields the one-frequency matching procedure used in [18].) After having so determined τ, one can uniquely define a corresponding best-fit phase shift $\alpha(\omega_1, \omega_2)$ by requiring that, say, $\phi'^{\rm EOB}_{22}(t'^{\rm EOB}_1) \equiv \phi^{\rm EOB}_{22}(t'^{\rm EOB}_1) + \alpha = \phi^{\rm NR}_{22}(t^{\rm NR}_1)$.

Having so related the EOB time and phase variables to the NR ones, we can straightforwardly compare all the EOB time series to their NR correspondents. In particular, we can compute the (shifted) EOB–NR phase difference

$$\Delta^{\omega_1,\omega_2}\phi^{\rm EOBNR}_{22}(t_{\rm NR}) \equiv \phi'^{\rm EOB}_{22}(t'^{\rm EOB}) - \phi^{\rm NR}_{22}(t^{\rm NR}). \tag{11}$$

In the following we will choose two matching instants (and corresponding frequencies) that take place during late inspiral and plunge, namely, $t^{\rm NR}_1 = 999.72$, $t^{\rm NR}_2 = 1494.94$ corresponding to $\omega_1 = 0.068\,15$, $\omega_2 = 0.2457$ (all expressed in M units).

To numerically implement the EOB/NR comparison we need to choose some values for the various "flexibility parameters" of the EOB framework. We have summarized above what these parameters are, and we have already indicated the values we chose for some of them. Among the remaining ones that need to be chosen, the two most crucial ones are a_5 and $\nu_{\rm pole}$. Recently, Damour and Nagar have shown, by using some of the data published in [18], that the *inspiral waveform* (for GW frequencies smaller than about $0.14/M$) could be remarkably well matched by the EOB one if one chooses values of a_5 and $\nu_{\rm pole}$ following the rather precise correlation plotted in the upper panel of Fig. 3 in [24]. Here, as we are exploring a different physical regime (late inspiral, plunge, and coalescence, with GW frequencies mostly larger than about $0.1/M$), and comparing to a different set of numerical data, we shall not *a priori* impose the precise correlation between a_5 and $\nu_{\rm pole}$ found in [24]. However, we shall make use of some previous results suggesting a preferred range for the values of a_5. On the one hand, Ref. [23] showed that the *faithfulness* (in the sense of Sec. VI A of [27]) of (restricted) EOB waveforms against NASA-Goddard NR coalescence waveforms was largest when a_5 belonged to some rather wide interval (which also depended on the considered mass ratio). See Fig. 2 (right panel) in [23] from which one might conclude that a_5 lies probably between $\sim$10 and $\sim$100. Buonanno *et al.* then chose $a_5 = 60$ as the

[9] As mentioned in Sec. II, we use the waveform extracted at a (coordinate) radius $R_{\rm NR} = 120M_c \simeq 120M$, and $t_{\rm NR}$ is the time of the "observer" located at the latter radius.

[10] Alternatively, one can start by giving oneself ω_1, ω_2 and determine the NR instants $t^{\rm NR}_1$, $t^{\rm NR}_2$ at which they are reached.

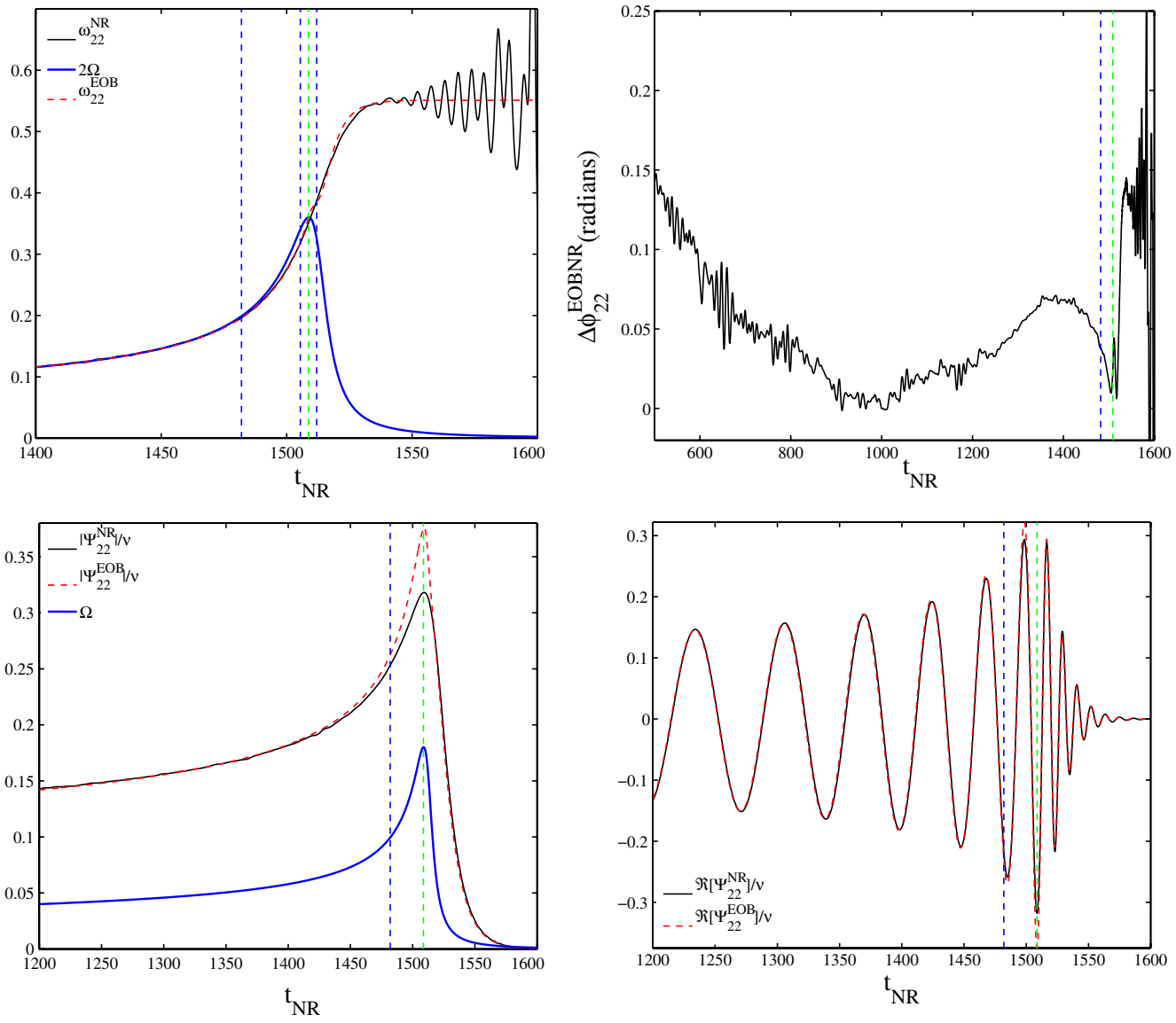

FIG. 1 (color online). Comparison between EOB and NR waveforms for $a_5 = 25$ and $v_{\rm pole} = 0.6241$: frequencies (top-left panel), phase difference (top-right panel), amplitudes (bottom-left panel), and real parts (bottom-right panel) of the two gravitational waveforms. The vertical line at $t_{\rm NR} = 1509$ locates the maximum of (twice) the orbital frequency Ω (alias the EOB light ring) and indicates the center of our matching comb (whose total width is indicated by the two neighboring vertical lines in the top-left panel). The vertical dashed line at $t^{\rm NR} = 1482$ indicates the crossing time of the adiabatic LSO orbital frequency ($\Omega_{\rm LSO} = 0.1003$).

"best-fit" value. On the other hand, Ref. [24] found that the phase agreement between (resummed) EOB waveforms and a rather long inspiral NR waveform was at its best when a_5 lied in a similarly wide interval (between $\sim$10 and $\sim$80) centered around $a_5 \sim 40$. In view of these results we shall focus, in the following, on two representative values of a_5, namely, $a_5 = 25$ (representative of the leftward side of preferred a_5 values), and $a_5 = 60$ (representative of the rightward side of preferred a_5 values, and chosen as best value by [23]). We have also checked that the values of a_5 between 25 and 60 lead (with an appropriate choice of $v_{\rm pole}$) to results that are at least as good as the ones we shall exhibit below.

A. Comparing NR to resummed EOB for $a_5 = 25$

At this stage we have essentially fixed all the flexibility of the EOB formalism apart from the choices of $v_{\rm pole}$, and of the comb spacing δ. Among these two parameters, only the former one, $v_{\rm pole}$, is important for getting a very accurate phase agreement between EOB and NR. When $a_5 = 25$, we found (by trial and error) that[11] $v_{\rm pole} = 0.6241$

[11]Though we did not investigate thoroughly what "error bar" can be put on such a "best" value of $v_{\rm pole}$, the numerical studies that we performed indicate that a change of ± 2 on the last (i.e. fourth) digit that we quote is sufficient to entail a visible worsening of the phase difference $\Delta\phi_{22}^{\rm EOBNR}$.

(together with $\delta = 1.7M_{\rm f}$ which is, however, less crucial) yields an excellent EOB/NR agreement. We exhibit our results in the four panels of Fig. 1.

The top-left panel of Fig. 1 compares the NR GW frequency both to the (matched) EOB GW frequency and to twice the orbital frequency. The time axis is $t_{\rm NR}$, and/or (see above) $t'_{\rm EOB} = t_{\rm EOB} + \tau$ (with $\tau = -2032M$ for the present case). The vertical lines on the right indicate the center and the outlying ''teeth'' of our matching comb, which is, as explained above, centered on the maximum of the EOB orbital frequency (also called EOB light ring). The interval between the two vertical lines [last stable orbit (LSO) and EOB light ring] defines the ''plunge.'' The dashed vertical line on the left (at $t_{\rm NR} = 1482$) indicates the crossing time of the adiabatic last stable orbit (ω-LSO in the sense of [3]). Note that the three frequencies are initially close to each other, but that, later, 2Ω separates from $\omega_{22}^{\rm NR}$ and $\omega_{22}^{\rm EOB}$, which continue to be in very close agreement, except for a slight discrepancy around merger, which, within the EOB approach, is conventionally supposed to take place at the maximum of Ω. Note also the good agreement between the EOB GW frequency during the ring-down plateau and the average of the NR one. As discussed in Sec. II the values for the mass and dimensionless spin of the final black hole that we used (together with [52]) to compute the QNMs frequencies are $M_{\rm f}^{\rm ring} = 0.959\,165M$, $j_{\rm f}^{\rm ring} = 0.684\,639$.

The top-right panel of Fig. 1 shows the EOB-NR phase difference, Eq. (11) (pinched at the two instants, $t_1^{\rm NR}$, $t_2^{\rm NR}$, given above). It is remarkable that the (two-sided[12]) EOB-NR phase difference over the time interval $(639M, 1524M)$ (which covers about 12 GW cycles of inspiral, plunge, and early ring-down) is smaller than about $\pm\frac{1}{2}0.068$ radians, which corresponds to ± 0.005 GW cycles.

The bottom-left panel of Fig. 1 compares the NR GW amplitude to the resummed 3^{+2}-PN-accurate EOB one. It also shows the orbital frequency Ω as an aid to locate the merger. One notices a very good agreement between the two amplitudes. During the interval $(1100M, 1400M)$ the fractional EOB-NR amplitude difference varies between -1% and $+1\%$. After $t_{\rm NR} = 1400M$, this fractional difference increases from $+1\%$ to a maximum of $+18\%$ (reached at $t_{\rm NR} \simeq 1509M$) and then decreases to take values of order -5% during the observationally relevant part of the ring-down. Note also that the NR equal-mass amplitude (divided by ν, i.e. by μ) time series is qualitatively, and even quantitatively, very similar to the corresponding NR test-mass amplitude time series shown in Fig. 3 of [22]. For instance, the value of the maximum amplitude is ~ 0.3 in both cases. A similar qualitative, but *not* quantitative, parallelism exists for the two corresponding frequency time series (the $\nu = 1/4$ frequency leveling off at a higher ''plateau'').

Finally, the bottom-right panel of Fig. 1 compares the real parts of the NR and EOB waveforms. The two vertical lines delimit the interval between the LSO and EOB light ring. Again the agreement between the two waveforms is impressive. Note that this last panel shows only the late inspiral, plunge, and ring-down. From the panel showing the phase difference, one can gather that the agreement stays as impressive over a much longer time span of order $1000M$ (essentially from $t_{\rm NR} \sim 500M$ to the end of ring-down).

B. Comparing NR to resummed EOB for $a_5 = 60$

Let us now consider our second representative value of the effective 4PN radial potential parameter, $a_5 = 60$. As before, we chose $\delta = 1.7M_{\rm f}$. We also selected the same phase pinching interval as above. Then, by trial and error, we found that $v_{\rm pole} = 0.5356$ yields an excellent EOB/NR agreement.[13]

We exhibit our results in the four panels of Fig. 2, which are entirely parallel to those of Fig. 1. The remarkable level of EOB/NR agreement that we get now, when $a_5 = 60$, is rather close to the one that we got above when $a_5 = 25$. At this stage, there is no rationale for saying that either value of a_5 is preferred over the other (though $a_5 = 25$ yields somewhat better results). Some partial numerical tests that we performed suggest that this conclusion extends to (at least) all values of a_5 between 25 and 60.

Some of the numbers quantifying the EOB/NR agreement are as follows:

(i) The (two-sided) EOB-NR phase difference over the time interval $(500M, 1550M)$ (which covers about 13 GW cycles of inspiral, plunge, and most of the ring-down) is smaller than about $\pm\frac{1}{2}0.13$ radians, which corresponds to ± 0.01 GW cycles.

(ii) During the interval $(1100M, 1400M)$ the fractional EOB-NR amplitude difference varies between -0.8% and $+0.55\%$. After $t_{\rm NR} = 1400M$, this fractional difference increases from $+0.55\%$ to a maximum of $+23\%$ (reached at $t_{\rm NR} \simeq 1511M$) and then decreases to take values of order $+6\%$ during the observationally relevant part of the ring-down.

C. Contrasting resummed EOB with restricted EOB, for $a_5 = 60$, by comparing NR to a standard restricted-EOB waveform

Finally, we wish to illustrate the importance (for reaching a high level of accuracy) of the various ingredients used

[12] As the reference level of any phase difference $\Delta\phi$ is arbitrary, it is convenient to use a ''middle'' reference level such that $\Delta\phi(t)$ varies between $-\varepsilon$ and $+\varepsilon$ over the considered interval. We refer to $\pm\varepsilon = \pm 1/2[\max(\Delta\phi) - \min(\Delta\phi)]$ as the *two-sided* phase difference.

[13] Note that this best value of $v_{\rm pole}$ (for $a_5 = 60$ and $\nu = 1/4$) happens to be numerically close to the best fitting $v_{\rm pole} \simeq 0.53$ value that Ref. [24] found in the test-mass limit $\nu \to 0$.

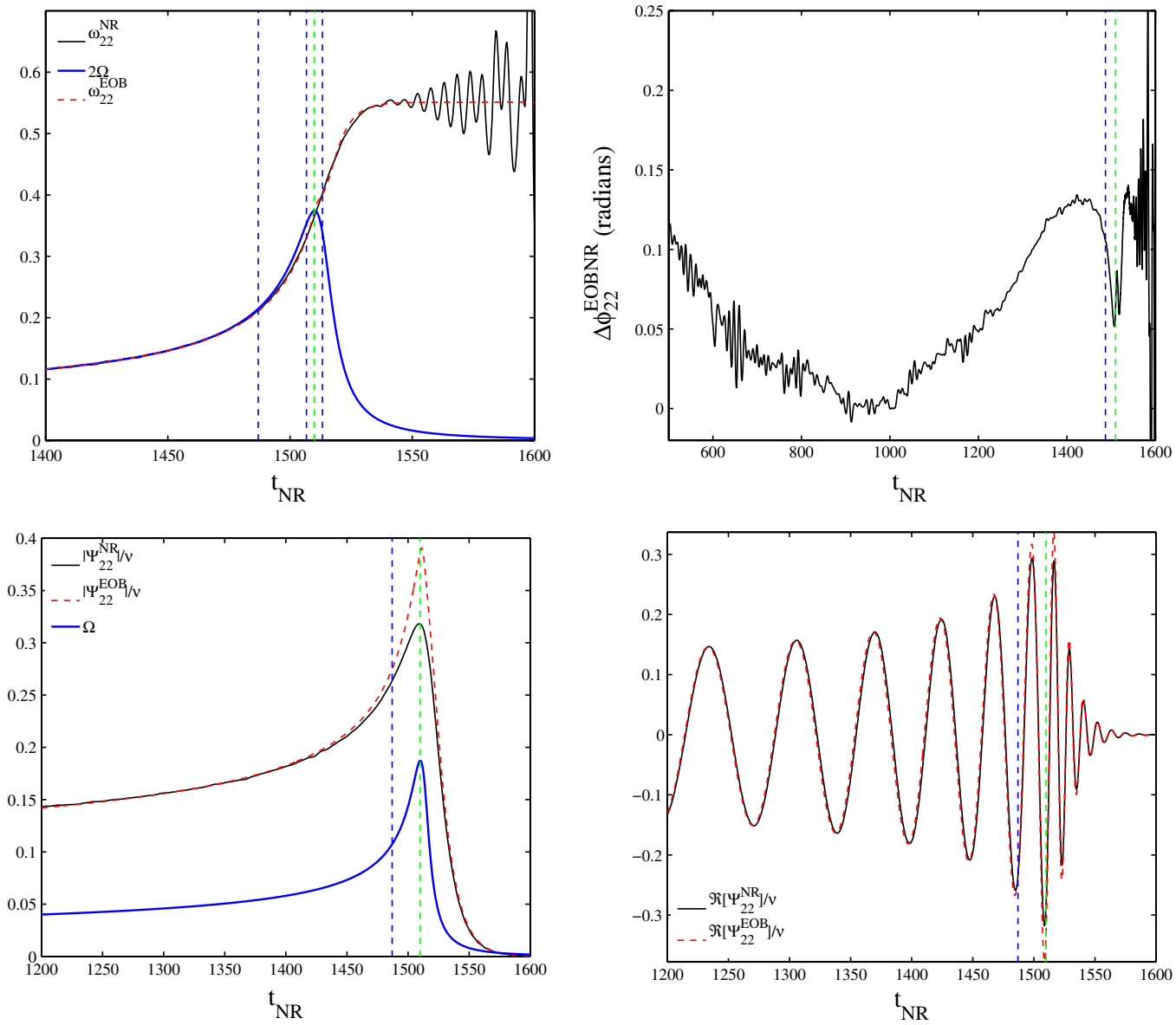

FIG. 2 (color online). Comparison between EOB and NR waveforms for $a_5 = 60$, $\nu_{\rm pole} = 0.5356$: frequencies (top-left panel), phase difference (top-right panel), amplitudes (bottom-left panel), and real parts (bottom-right panel) of the two gravitational waveforms. The vertical line at $t_{\rm NR} = 1510$ locates the maximum of (twice) the orbital frequency Ω (alias the EOB light ring) and indicates the center of our matching comb (whose total width is indicated by the two neighboring vertical lines in the top-left panel). The vertical dashed line at $t^{\rm NR} = 1487$ indicates the crossing time of the adiabatic LSO orbital frequency ($\Omega_{\rm LSO} = 0.1081$).

in our present, resummed version of EOB (using a time-extended ''comb matching'' to 5 QNMs) by comparing NR to the type of simpler implementation of the EOB framework used in [23]. Using again $a_5 = 60$ (which was chosen as best value in [23]), we compare NR to the following implementation of EOB:

(i) We use for $\nu_{\rm pole}$ the standard value $\nu_{\rm pole}^{\rm DIS}(\nu)$ advocated in [1].

(ii) We use (as originally proposed in Ref. [3]) the following (Newtonian-order and Kepler-law-assuming) restricted quadrupole waveform,

$$\Psi_{22}^{\rm NK}(t) = -4\nu\sqrt{\frac{\pi}{30}}\Omega^{2/3}\exp(-2i\Phi), \qquad (12)$$

without any explicit PN (F_{22}) corrections, nor any NQC (a, b) corrections.

(iii) We use only 3 (positive-frequency) QNMs.

(iv) And, we match the plunge and ring-down waveforms in a very small interval ($\delta/M_{\rm f} = 0.2$ instead of our preferred 1.7) around the maximum of the orbital frequency. (Indeed, the matching of the two waveforms and their derivatives at a sharply defined mo-

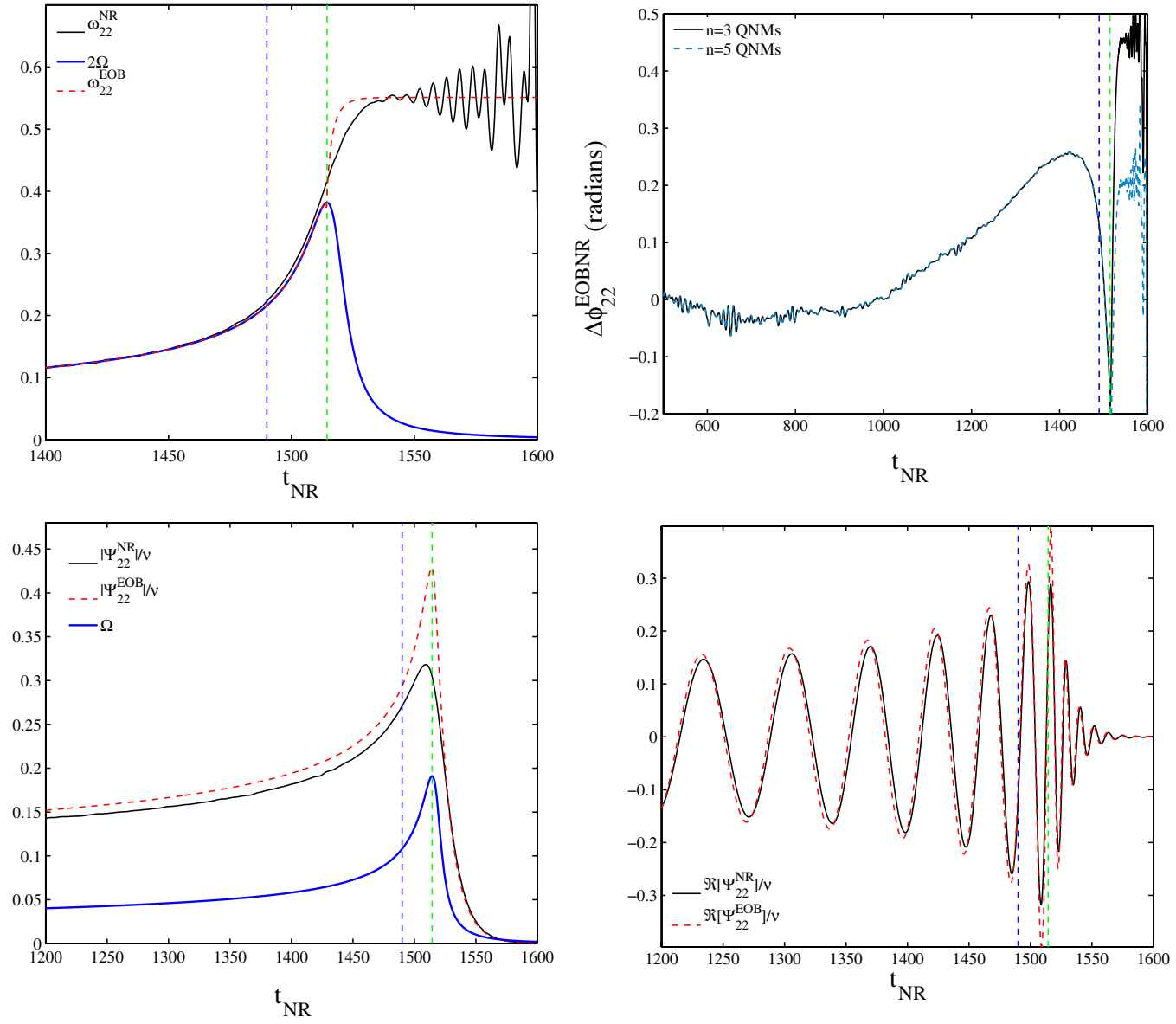

FIG. 3 (color online). Comparison between the EOB restricted waveform approximation, Eq. (12), and NR for $a_5 = 60$ and $v_{\rm pole} = v_{\rm pole}^{\rm DIS}(\nu = 1/4) = 0.6907$: frequencies (top-left panel), phase difference (top-right panel), amplitudes (bottom-left panel), and real parts (bottom-right panel) of the two gravitational waveforms. The vertical line at $t_{\rm NR} = 1510$ locates the maximum of (twice) the orbital frequency Ω (alias the EOB light ring) and indicates the matching time. The vertical dashed line at $t^{\rm NR} = 1490$ indicates the crossing time of the adiabatic LSO orbital frequency ($\Omega_{\rm LSO} = 0.1081$).

ment is equivalent to considering the $\delta \to 0$ limit of our comb-matching technique.)

The results of such a coarser EOB implementation are shown in Fig. 3 (which is parallel to the previous two figures). By contrasting Fig. 3 with Fig. 2 (which used the *same value* of a_5), we see that

(i) the EOB frequency agrees less well with the NR one than before, especially around the matching point. Note, in particular, that the post-matching analytical frequency jumps up from the maximum (doubled) orbital frequency significantly more vertically than before, thereby decoupling too soon from the exact frequency, and accruing a larger dephasing than before (because of the too-localized matching, and—to a lesser degree—the use of only 3 QNMs).

(ii) The EOB-NR (maximal) phase difference over the same time interval ($500M$, $1524M$) is about 2.2 times larger than before. One now ends up with a phase difference of $\pm\frac{1}{2}0.29$ radians, i.e. 0.023 GW cycles over about 13 GW cycles. The top-right panel of Fig. 3 illustrates the fact that matching with 5 QNMs (dashed line) reduces the dephasing accumulated during the transition from merger to ring-down.

(iii) The modulus of the analytical waveform is now distinctly larger than the NR one during the inspiral (because of the lack of PN corrections).
(iv) The modulus also exhibits a more significant discrepancy (+ 35%) with the NR one at the end of the plunge (because of the use of the Kepler-law-assuming $\propto \Omega^{2/3}$, which, as pointed out in [25], tends to overestimate the amplitude).
(v) Note also that one visually notices these differences at the level of the GW waveforms.
(vi) The same resummed-EOB/restricted-EOB comparison was done in [22], in the $\nu \ll 1$ case, with similar conclusions.

In spite of these relative blemishes, note, however, that this "coarser" EOB-type implementation still succeeds in following the phase of the exact signal to ± 0.023 GW cycles over about 13 GW cycles.

Note that the corresponding EOB/NR agreement exhibited in Fig. 4 of Ref. [23] seems to be somewhat better[14] than the one exhibited by our Fig. 3. This difference might have several origins, notably, (i) a difference in the accuracy of the NR data,[15] and (ii) a difference in the procedure used to best shift time and phase between EOB and NR data.

V. CONCLUSIONS

We have compared a recently proposed, resummed 3^{+2}-PN-accurate EOB waveform to the result of a numerical simulation of a coalescing equal-mass binary black hole performed at the Albert Einstein Institute. We find a remarkable agreement, both in phase and in amplitude, between the new EOB waveform and the numerical data. More precisely, we find that the maximal dephasing between EOB and NR can be reduced below ± 0.005 GW cycles over the last $\sim 900M$ (corresponding to about 12 GW cycles plus ring-down ones) of the simulation. This level of agreement was exhibited for two representative values of the effective 4PN parameter a_5, namely, $a_5 = 25$ and $a_5 = 60$, and for a corresponding, appropriately flexed value of the radiation-reaction resummation parameter $v_{\rm pole}$. In addition, our resummed-EOB amplitude agrees to better than the 1% level with the NR one up to the late inspiral.

We have also compared the NR data to a coarser implementation of the EOB approach (restricted waveform, standard $v_{\rm pole}^{\rm DIS}$, instantaneous matching to 3 QNMs). The EOB/NR agreement is slightly less good in this case, though the phase agreement remains quite good ($\pm$ 0.023 GW cycles over the last $\sim 1000M$ of the simulation).

Let us point out a notable feature of our results. In the recent work of Damour and Nagar [24], the same resummed 3^{+2}-PN-accurate EOB waveform was compared to a long, very accurate equal-mass inspiral simulation of the Caltech-Cornell group [18]. It was found that an excellent EOB/NR agreement was obtained when a_5 and $v_{\rm pole}$ were following the rather precise correlation plotted in the upper panel of Fig. 3 of Ref. [24]. Let us denote this correlation as $a_5 \to v_{\rm pole}^{\rm best\ inspiral}(a_5)$. In the present paper, we similarly found that the EOB/NR agreement was at its best when, for a given a_5,[16] $v_{\rm pole}$ was taking a rather precise corresponding best-fit value, say, $v_{\rm pole}^{\rm best\ insplunge}(a_5)$. In particular, we found $v_{\rm pole}^{\rm best\ insplunge}(25) = 0.6241$ and $v_{\rm pole}^{\rm best\ insplunge}(60) = 0.5356$. On the other hand, the results of [24] yield $v_{\rm pole}^{\rm best\ inspiral}(25) = 0.5340$ and $v_{\rm pole}^{\rm best\ inspiral}(60) = 0.4856$. The differences between these sets of values are $v_{\rm pole}^{\rm best\ insplunge}(25) - v_{\rm pole}^{\rm best\ inspiral}(25) = 0.0901$ and $v_{\rm pole}^{\rm best\ insplunge}(60) - v_{\rm pole}^{\rm best\ inspiral}(60) = 0.0500$. Note also that the "best insplunge" $v_{\rm pole}$ values are in between the "best inspiral" ones and the originally advocated [1] one $v_{\rm pole}^{\rm DIS}(\nu = 1/4) = 0.6907$. This finding will deserve further investigation in the future. At this stage we can only speculate on the various possible origins of this difference: (i) it might be due to the fact that, not having access to the original NR data of [18], Damour and Nagar had to rely on rather coarse measurements extracted from published figures; (ii) it might be due to systematic errors in the NR data of [18]; (iii) it might alternatively come from systematic errors in the NR data used in the present paper; (iv) it might come from the fact that the best-fit $\mathcal{F}_\varphi(v_{\rm pole})$ is not a uniform approximation (as a function of frequency) to the exact radiation reaction (see, in the $\nu \to 0$ limit, the bottom panels of Fig. 1 in [24]), and finally, (v) it might come from some "missing physics" in the resummed-EOB waveform explored here. There are several candidates for this missing physics. One suggestion (which follows the original suggestion of [5]) is that one might need to consider still higher (uncalculated) PN contributions to the radial EOB potential[17] $A(u) = 1 - 2u + 2\nu u^3 + a_4 \nu u^4 + a_5 \nu u^5 + a_6 \nu u^6 + \cdots$ where $u = 1/r$. Another suggestion is that NQC corrections to radiation reaction might modify the phasing during late inspiral and plunge. As an example, we have looked at this possibility.

[14]The reader should, however, keep in mind that in Fig. 4 of Ref. [23] the EOB-NR phase difference is divided by 2π compared to the one shown in our Fig. 3.

[15]The data used in [23] did not benefit from the reduction in eccentricity used in the data considered here.

[16]Though we did not explore all possible values of a_5, we sampled intermediate values between the representative a_5 values we picked and convinced ourselves that the same conclusion held for them.

[17]For simplicity, we consider only linear-in-ν higher PN contributions. If the need arises (and the fact that the unequal-mass EOB/NR comparisons of [23] seem to exhibit a strong dependence on the mass ratio might suggest it) one can easily add in a nonlinear ν dependence.

More precisely, following [22], we can introduce a new flexibility parameter $\bar{a}^{\rm RR}$[18] such that the radiation-reaction force is multiplied by a correction factor $f_{\rm RR}^{\rm NQC}$ given by

$$f_{\rm RR}^{\rm NQC} = \left(1 + \bar{a}^{\rm RR}\frac{p_{r_*}^2}{(r\Omega)^2 + \epsilon}\right)^{-1}. \qquad (13)$$

Such a factor will be very close to 1 during the inspiral (and therefore will be negligible in the EOB comparison to the Caltech-Cornell data), but will start being significantly less than 1 (if $\bar{a}^{\rm RR} > 0$) during the late inspiral and plunge, which are of interest for the comparison to the presently considered data. And indeed, we have found that by choosing a value $\bar{a}^{\rm RR} \sim +40$ (and $\epsilon = 0.12$ as in the waveform NQC factor considered above) we could, when $a_5 = 25$, obtain an excellent EOB/NR fit by using the ''best inspiral'' value $\nu_{\rm pole}^{\rm best\ inspiral}(25) = 0.5340$ (instead of the above $\nu_{\rm pole}^{\rm best\ insplunge}(25) = 0.6241$). This issue needs to be further investigated by using the most accurate possible data covering both inspiral and plunge. We hope to come back to it in the future.

[18]Actually [22] introduced a parameter $a^{\rm RR}$ which is, roughly, the negative of $\bar{a}^{\rm RR}$, with a NQC radiation-reaction factor of the form $1 + a^{\rm RR}p_{r_*}^2/(r\Omega)^2$.

Finally, we think that the present work, taken in conjunction with other recent works on the EOB/NR comparison, confirms the ability of the EOB formalism to accurately capture the general-relativistic waveforms. The present work has also shown that the recently proposed resummed 3^{+2}-PN-accurate waveform is important for defining analytical EOB waveforms that faithfully represent (both in phase and in amplitude) the waveforms emitted by equal-mass coalescing (nonspinning) black-hole binaries.

ACKNOWLEDGMENTS

We thank Peter Diener for assistance and discussion in the early stages of this work, Sascha Husa for help with the NR initial data, and Sebastiano Bernuzzi for help in the analysis of the ring-down waveform. The NR computations were performed with the Damiana, Belladonna, and Peyote clusters of the Albert Einstein Institute. This work was supported in part by DFG Grant No. SFB/Transregio 7 ''Gravitational Wave Astronomy.'' The activity of A. N. at IHES is supported by INFN. The commercial software products MATHEMATICA and MATLAB have been extensively used in the preparation of this paper.

[1] T. Damour, B. R. Iyer, and B. S. Sathyaprakash, Phys. Rev. D **57**, 885 (1998).
[2] A. Buonanno and T. Damour, Phys. Rev. D **59**, 084006 (1999).
[3] A. Buonanno and T. Damour, Phys. Rev. D **62**, 064015 (2000).
[4] T. Damour, P. Jaranowski, and G. Schaefer, Phys. Rev. D **62**, 084011 (2000).
[5] T. Damour, Phys. Rev. D **64**, 124013 (2001).
[6] A. Buonanno, Y. Chen, and T. Damour, Phys. Rev. D **74**, 104005 (2006).
[7] F. Pretorius, Phys. Rev. Lett. **95**, 121101 (2005).
[8] M. Campanelli, C. O. Lousto, P. Marronetti, and Y. Zlochower, Phys. Rev. Lett. **96**, 111101 (2006).
[9] M. Campanelli, C. O. Lousto, and Y. Zlochower, Phys. Rev. D **74**, 041501(R) (2006).
[10] J. G. Baker, J. Centrella, D. I. Choi, M. Koppitz, and J. van Meter, Phys. Rev. D **73**, 104002 (2006).
[11] J. G. Baker, J. Centrella, D. I. Choi, M. Koppitz, J. R. van Meter, and M. C. Miller, Astrophys. J. **653**, L93 (2006).
[12] J. G. Baker, M. Campanelli, F. Pretorius, and Y. Zlochower, Classical Quantum Gravity **24**, S25 (2007).
[13] J. A. Gonzalez, U. Sperhake, B. Brügmann, M. Hannam, and S. Husa, Phys. Rev. Lett. **98**, 091101 (2007).
[14] S. Husa, J. A. Gonzalez, M. Hannam, B. Brugmann, and U. Sperhake, arXiv:0706.0740.
[15] M. Koppitz, D. Pollney, C. Reisswig, L. Rezzolla, J. Thornburg, P. Diener, and E. Schnetter, Phys. Rev. Lett. **99**, 041102 (2007).
[16] L. Rezzolla, E. N. Dorband, C. Reisswig, P. Diener, D. Pollney, E. Schnetter, and B. Szilagyi, arXiv:0708.3999.
[17] L. Rezzolla, P. Diener, E. N. Dorband, D. Pollney, C. Reisswig, E. Schnetter, and J. Seiler, arXiv:0710.3345 [Astrophys. J. (to be published)].
[18] M. Boyle, D. A. Brown, L. E. Kidder, A. H. Mroué, H. P. Pfeiffer, M. A. Scheel, G. B. Cook, and S. A. Teukolsky, Phys. Rev. D **76**, 124038 (2007).
[19] A. Buonanno, G. B. Cook, and F. Pretorius, Phys. Rev. D **75**, 124018 (2007).
[20] Y. Pan *et al.*, Phys. Rev. D **77**, 024014 (2008).
[21] T. Damour and A. Nagar, Phys. Rev. D **76**, 044003 (2007).
[22] T. Damour and A. Nagar, Phys. Rev. D **76**, 064028 (2007).
[23] A. Buonanno, Y. Pan, J. G. Baker, J. Centrella, B. J. Kelly, S. T. McWilliams, and J. R. van Meter, Phys. Rev. D **76**, 104049 (2007).
[24] T. Damour and A. Nagar, Phys. Rev. D **77**, 024043 (2008).
[25] T. Damour and A. Gopakumar, Phys. Rev. D **73**, 124006 (2006).
[26] A. Nagar, T. Damour, and A. Tartaglia, Classical Quantum Gravity **24**, S109 (2007).
[27] T. Damour, B. R. Iyer, P. Jaranowski, and B. S. Sathyaprakash, Phys. Rev. D **67**, 064028 (2003).
[28] T. Damour, E. Gourgoulhon, and P. Grandclement, Phys. Rev. D **66**, 024007 (2002).

[29] P. Ajith *et al.*, Classical Quantum Gravity **24**, S689 (2007).
[30] P. Ajith *et al.*, arXiv:0710.2335 [Phys. Rev. D (to be published)].
[31] D. Pollney *et al.*, Phys. Rev. D **76**, 124002 (2007).
[32] T. Goodale, G. Allen, G. Lanfermann, J. Massó, T. Radke, E. Seidel, and J. Shalf, in *VECPAR'2002, 5th International Conference*, Lecture Notes in Computer Science (Springer, Berlin, 2003).
[33] C. Bona, J. Masso, E. Seidel, and J. Stela, Phys. Rev. Lett. **75**, 600 (1995).
[34] M. Alcubierre, B. Brugmann, P. Diener, M. Koppitz, D. Pollney, E. Seidel, and R. Takahashi, Phys. Rev. D **67**, 084023 (2003).
[35] J. G. Baker, J. Centrella, D. I. Choi, M. Koppitz, and J. van Meter, Phys. Rev. Lett. **96**, 111102 (2006).
[36] E. Schnetter, S. H. Hawley, and I. Hawke, Classical Quantum Gravity **21**, 1465 (2004).
[37] J. Thornburg, Classical Quantum Gravity **21**, 743 (2004).
[38] A. Nagar and L. Rezzolla, Classical Quantum Gravity **22**, R167 (2005); **23**, 4297(E) (2006).
[39] D. R. Brill and R. W. Lindquist, Phys. Rev. **131**, 471 (1963).
[40] S. Brandt and B. Brugmann, Phys. Rev. Lett. **78**, 3606 (1997).
[41] M. Ansorg, B. Brugmann, and W. Tichy, Phys. Rev. D **70**, 064011 (2004).
[42] G. B. Cook, Phys. Rev. D **50**, 5025 (1994).
[43] H. P. Pfeiffer, D. A. Brown, L. E. Kidder, L. Lindblom, G. Lovelace, and M. A. Scheel, Classical Quantum Gravity **24**, S59 (2007).
[44] S. Husa, M. Hannam, J. A. Gonzalez, U. Sperhake, and B. Brugmann, Phys. Rev. D **77**, 044037 (2008).
[45] T. Damour, P. Jaranowski, and G. Schafer, Phys. Lett. B **513**, 147 (2001).
[46] L. Blanchet, T. Damour, G. Esposito-Farese, and B. R. Iyer, Phys. Rev. Lett. **93**, 091101 (2004).
[47] O. Dreyer, B. Krishnan, D. Shoemaker, and E. Schnetter, Phys. Rev. D **67**, 024018 (2003).
[48] A. Ashtekar and B. Krishnan, Phys. Rev. D **68**, 104030 (2003).
[49] E. N. Dorband, E. Berti, P. Diener, E. Schnetter, and M. Tiglio, Phys. Rev. D **74**, 084028 (2006).
[50] E. Berti, V. Cardoso, J. A. Gonzalez, and U. Sperhake, Phys. Rev. D **75**, 124017 (2007).
[51] E. Berti, V. Cardoso, J. A. Gonzalez, U. Sperhake, M. Hannam, S. Husa, and B. Bruegmann, Phys. Rev. D **76**, 064034 (2007).
[52] E. Berti, V. Cardoso, and C. M. Will, Phys. Rev. D **73**, 064030 (2006).
[53] M. Davis, R. Ruffini, and J. Tiomno, Phys. Rev. D **5**, 2932 (1972).
[54] L. Blanchet, T. Damour, B. R. Iyer, C. M. Will, and A. G. Wiseman, Phys. Rev. Lett. **74**, 3515 (1995).
[55] L. Blanchet, B. R. Iyer, and B. Joguet, Phys. Rev. D **65**, 064005 (2002); **71**, 129903(E) (2005).
[56] L. Blanchet, T. Damour, G. Esposito-Farese, and B. R. Iyer, Phys. Rev. Lett. **93**, 091101 (2004).
[57] L. Blanchet, T. Damour, G. Esposito-Farese, and B. R. Iyer, Phys. Rev. D **71**, 124004 (2005).
[58] L. Blanchet, G. Faye, B. R. Iyer, and B. Joguet, Phys. Rev. D **65**, 061501 (2002); **71**, 129902(E) (2005).
[59] H. Tagoshi and M. Sasaki, Prog. Theor. Phys. **92**, 745 (1994).
[60] L. E. Kidder, Phys. Rev. D **77**, 044016 (2008).
[61] W. H. Press and S. A. Teukolsky, Astrophys. J. **185**, 649 (1973).
[62] H. Onozawa, Phys. Rev. D **55**, 3593 (1997).